AUTHOR-FORMATTED ACCEPTED VERSION

Electrophoretic Molecular Communication with Time-Varying Electric Fields

Sunghwan Cho[a,b], Thomas C. Sykes[a,*], Justin P. Coon[a], Alfonso A. Castrejón-Pita[a]

[a]*Department of Engineering Science, University of Oxford, Oxford, OX1 3PJ, UK*
[b]*Department of Electrical Engineering, Korea Military Academy, Seoul, 01805, Republic of Korea*

Abstract

This article investigates a novel electrophoretic molecular communication framework that utilizes a time-varying electric field, which induces time-varying molecule velocities and in turn improves communication performance. For a sinusoidal field, we specify favorable signal parameters (e.g., phase and frequency) that yield excellent communication-link performance. We also analytically derive an optimized field function by formulating an appropriate cost function and solving the Euler-Lagrange equation. In our setup, the field strength is proportional to the molecular velocity; we verify this assumption by solving the Basset-Boussinesq-Oseen equation for a given time-varying electric field (forcing function) and examining its implications for practical physical parameterizations of the system. Our analysis and Monte-Carlo simulation results demonstrate that the proposed time-varying approach can significantly increase the number of information-carrying molecules expected to be observed at the receiver and reduce the bit-error probability compared to the constant field benchmark.

Keywords: molecular communication, electrophoresis, microfluidics, biomimetic communication, fluid dynamics, nanonetworks

1. Introduction

In the last decade, there have been considerable advancements in nanonetworks, consisting of nano-scale functional components that can perform very simple and specific tasks, such as sensing, actuation, computing, and data storage [1]. The interconnection of these *nanomachines* allows individual components' limitations to be overcome in nanonet-

---

*Corresponding author

Email addresses: scho@kma.ac.kr (Sunghwan Cho), thomas.sykes@eng.ox.ac.uk, t.c.sykes@outlook.com (Thomas C. Sykes), justin.coon@eng.ox.ac.uk (Justin P. Coon), alfonso.castrejon-pita@wadham.ox.ac.uk (Alfonso A. Castrejón-Pita)

works, thus expanding nanomachines' capabilities by providing them with a way to co-operate and share information. The resulting nanonetworks' potential applications are vast and varied, including industrial and consumer goods, environmental applications, biomedical sciences, and defence [2]. The key challenge in exploiting nanonetworks in such applications is introducing an effective communication mechanism between the constituent nanomachines. However, there are emerging applications in which conventional radio frequency communication technologies are unsafe or impractical, so there is a requirement to explore alternative communication mediums (including optical, acoustic and mechanical) or to define entirely new paradigms, such as those inspired by biology [3].

In nature, various cells and living organisms exchange information employing molecular communication (MC); that is, they use molecules as biochemical signals to encode, transmit and receive information [4, 5]. For example, hormones transmit signals within multicellular organisms, whereas pheromones are secreted to communicate with members of the same species [6]. Motivated by natural MC systems refined by evolution over countless millennia, biomimetic engineered applications exploiting MC have gained increasing attention within the communications research community as a potential communication solution for nanonetworks, kick-starting highly-interdisciplinary research in this area [1]. Additional advantages of MC is that it is naturally biocompatible and consumes very little energy [7, 8].

At present, technical harnessing of molecular signaling in a fluid medium can be achieved in an engineered manner by exploiting the advection and diffusion of information-carrying molecules [9]. Transport by advection can be categorized as force-induced drift, where advection can be induced by external forces acting on the information-carrying molecules (not on the fluid molecules), and bulk flow, where movement of the fluid induces molecule motion. Without advection (i.e., a purely diffusive environment), a signal distortion in which one symbol interferes with subsequent symbols, called intersymbol interference (ISI), is a significant problem in MC, especially when the distance that molecules must travel is large. Hence, in the absence of advection, only low rates of transmission are generally achievable [6]. A means of molecule advection (e.g., fluid pumping) may already exist in MC systems, but can also be induced or otherwise harnessed to reduce ISI in a communication sense by migrating residual molecules (of previous symbols) away from the receiver.

On the one hand, existing literature concerning MC typically assumes the simplest case of steady and uniform advection, where 'steady' implies that the flow (i.e. velocity components) is not a function of time, whilst 'uniform' means that the fluid velocity is identical throughout the whole domain. Under the steady and uniform advection assumptions, various components of MC systems have been rigorously investigated [10–15].

On the other hand, utilizing bulk flow to propagate information-carrying molecules through a fluid medium to an intended receiver may not be suitable for applications where inducing a flow of the medium itself is problematic, unwanted, or even impossible – e.g., in lab-on-a-chip (LoC) devices employing microfluidics with highly-parallel arrays of reactors in which inlet and outlet ports must be shared among many chip components [16]. Electric fields can potentially be used as an alternative means to propagate information-carrying molecules, bringing with them an additional advantage of allowing

(depending on the fluid flow rate and applied electric field) the molecules to be propagated in a direction independent of any fluid flow that may already exist in the system. For neutrally-charged molecules, dielectrophoresis (the motion of neutrally-charged polarisable molecules subject to an asymmetric electric field) has been harnessed to enable increased data transmission rates in MC systems by maintaining bit ordering [17, 18]. However, this approach lacks the ability to controllably propagate information-carrying molecules themselves, since the electrodes are fixed and are merely switched on and off to either act as a buffer or a relay.

We suggest that the limitations of relying on dielectrophoresis or fluid flow alone can be overcome by using electric fields to directly influence the motion of individual charged molecules in a process known as electrophoresis. Electrophoresis is defined as the motion of dispersed particles relative to a fluid under the influence of a spatially uniform electric field [19] – see [20] for an introduction and comparison to dielectrophoresis. Note that electrophoresis can be readily achieved in LoC devices [21]. Used in this way, electric fields offer a degree of freedom that is inherently separate from molecular systems, where high field strengths can be used to propagate information-carrying molecules very quickly (low delay), and vice versa. The inherent advantages of electrophoresis leads us to contemplate that a time-varying electric field could further improve communication performance, including enabling higher data transmission rates and reducing bit error probabilities, which forms the basis of our proposed electrophoretic MC framework.

Our interest in the proposed electrophoretic framework extends beyond the communication framework in which it is cast though. Although molecules propagated by the electric field can be seen as bearers of information, they are simply reagents at the receiving site. In this context, the rate of communication is, to a degree, synonymous with the rate of reaction. Furthermore, we are concerned with the case where the "information" to be propagated through the fluid channel is unknown to both the transmitting end of the system as well as the receiving end. Such a scenario can arise in LoC applications, where compounds contained in a sample enter a particular part of the device and must be directed efficiently to one or more reaction sites. Hence, we believe that regulating the molecules' propagation with a degree of freedom via time-varying electric fields, while utilizing a communication theoretic framework to optimize this process, would bring numerous advantages in improving and developing such microfluidic device technologies. For instance, time-varying electric fields can be used to place sufficient numbers of different particles that chemically or biologically contain information at the corresponding measuring/sensing sites and at the desired times to improve the microfluidic devices' sensitivity and accuracy.

Herein, this exploratory study demonstrates the potential for enhanced communication performance under our proposed electrophoretic MC framework, whilst assessing its feasibility from several perspectives. The contributions of this work can be summarized as follows:

- alongside examining the physical mechanism of molecules' motion subject to time-varying electric fields in general, we investigate a specific sinusoidal field and propose a method to choose its signal parameters in order to increase the expected number
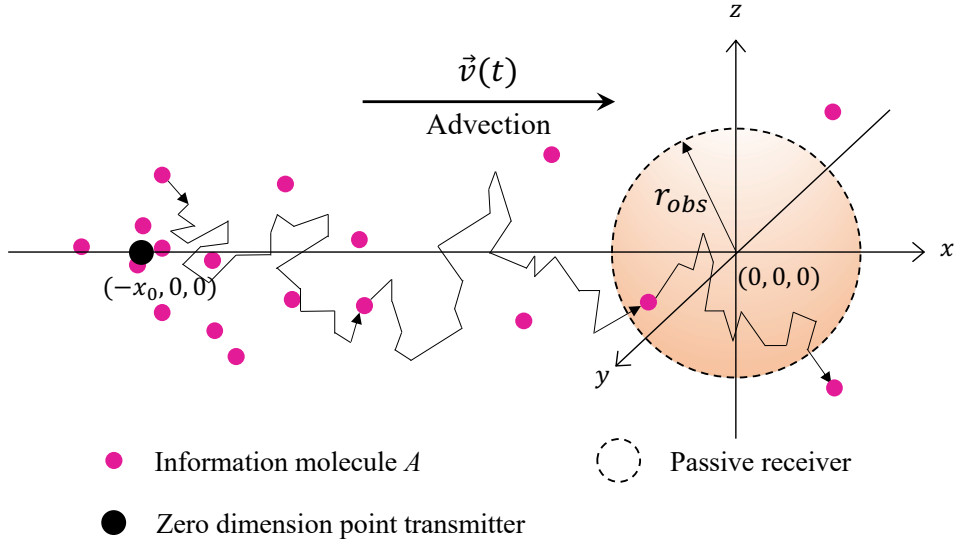
Figure 1. Schematic description of the system model, including a point transmitter, an infinite, three-dimensional channel, and a passive receiver sphere.

of information-carrying molecules within the receiver sphere when sampling occurs for a given bit interval;

- we analytically derive an optimized field (with exponential functional form) that minimises the mean squared error between the receiver location and the center of the transmitted molecule group, subject to a constraint on the average power of the electrical field;

- we show that the proposed electrophoresis framework is feasible from a fluid dynamics perspective by analyzing the effects of viscosity and mass on molecular motion in response to a time-varying electric field.

The rest of this paper is organized as follows. Section 2 introduces the system model describing the transmitter and receiver, the receiver signal model, and the detection scheme in MC systems. In Section 3, the sinusoidal and optimized fields are investigated in order to increase the expected number of molecules observed by the receiver. Section 4 explores the fluid dynamics underpinning electrophoretic molecular communication. Section 5 gives numerical and simulation results that support our analysis. Section 6 offers thoughts on future directions and section 7 concludes the paper.

2. System Model

In this section, we introduce the system model that is subsequently used to assess the efficacy of electrophoretic MC.

2.1. Transmitter and Receiver

The system model considered in this work is described in Fig. 1. The receiver is a sphere with radius r_{obs} and volume V_{obs}, which is fixed and centered at the origin (i.e.

the coordinate vector $\{0, 0, 0\}$, as defined by the orientation axes in Fig. 1) of an infinite, three-dimensional fluid environment of constant uniform temperature and viscosity. The receiver is a passive observer that does not impede the migration of molecules or initiate chemical reactions. The transmitter is a point source of information molecules (called A molecules) and fixed at $\{-x_0, 0, 0\}$. Note that this work considers a point transmitter and passive spherical receiver to simplify the MC system model, enabling us to focus on assessing the effect of utilizing electrophoresis. Extending this work to other types of transmitters (e.g., volume and ion-channel-based) and receivers (e.g., absorbing, reacting, optical, and conductivity-based) are interesting topics for future research.

Real MC systems can be impaired by A molecules that originate from interfering natural or synthetic sources, including other communication links in the same domain. We assume that the unintended noise and interference (in a communication sense) can be characterized as a Poisson random variable with a time-varying mean as in [12, 22].

The transmitter has a B-bit binary sequence $\mathbf{W} = \{W[1], W[2], \ldots, W[B]\}$ to send to the receiver, where $W[j]$ is the jth information bit and $\Pr(W[j] = 1) = P_1$. The transmitter uses binary modulation (i.e., only two symbols 0 and 1 are utilized) and transmission intervals of duration T_{int} seconds. To send a binary 1, N_{EM} molecules are released in an impulsive manner at the start of the bit interval to mitigate ISI. To send a binary 0, no molecules are released.

We assume that a time-varying electric field $\vec{E}(t)$ is applied uniformly over the entire environment. This field induces an electrophoretic force $\vec{F}_E(t) = q_A \vec{E}(t)$, which produces a flow of A molecules with time-varying velocity $\vec{v}(t)$, where q_A denotes the electric charge on a single A molecule. We assume that the molecule velocity is linearly related to the electrophoretic force, i.e., $\vec{v}(t) \propto \vec{E}(t)$. Section 4 will validate the applicability of this assumption and assess other possible effects on the molecules' motion. We define $\vec{v}(t)$ by its velocity component in each dimension, i.e. $\vec{v}(t) = \{v_x(t), v_y(t), v_z(t)\}$. The placement of the transmitter is such that $v_x(t)$ is positive in the direction of the receiver from the transmitter. Note that electrostatic repulsion between the like-charged molecules is not taken into account in this initial study.

2.2. Receiver Signal

The concentration of A molecules (transmitted at time t_0) at the point defined by vector $\vec{r}$ and at time t in molecule·m^{-3} is denoted by $C_A(\vec{r}, t; t_0)$ (or written as C_A for compactness). We assume that these molecules travel independently once they are released either by the transmitter or sources of noise. Due to the constant uniform temperature and viscosity of the environment, the A molecules diffuse with constant diffusion coefficient D_A (m^2/s). The differential equation describing the motion of A molecules due to both advection and diffusion (via Fick's second law [23]) is

$$\frac{\partial C_A}{\partial t} + \vec{v}(t) \cdot \nabla C_A = D_A \nabla^2 C_A, \tag{1}$$

where ∇ and ∇^2 denote the vector differential and Laplace operators, respectively. C_A can be interpreted as the expected point concentration due to an emission of N_{EM} molecules. By utilizing a moving reference frame for the time-varying flow with the initial condition

(IC) $C_A(\vec{r}, t_0; t_0) = N_{\text{EM}}\delta(\vec{r} - \vec{r}_{\text{TX}})$ and boundary condition (BC) $C_A(\vec{r} \to \infty, t; t_0) = 0$, the expected concentration at point $\{x, y, z\}$ for $t \geq t_0$ is

$$C_A(\vec{r}, t; t_0) = \frac{N_{\text{EM}}}{(4\pi D_A(t - t_0))^{3/2}} \exp\left(-\frac{|\vec{r}|^2}{4D_A(t - t_0)}\right), \tag{2}$$

dervied by integrating (1), where

$$|\vec{r}(t)|^2 = \left(x + x_0 - \int_{t_0}^{t} v_x(\tau)\,\mathrm{d}\tau\right)^2 + \left(y - \int_{t_0}^{t} v_y(\tau)\,\mathrm{d}\tau\right)^2 + \left(z - \int_{t_0}^{t} v_z(\tau)\,\mathrm{d}\tau\right)^2 \tag{3}$$

is the square of the *effective* distance from the transmitter at $\{-x_0, 0, 0\}$ to $\{x, y, z\}$.

The receiver is a passive observer, so the expected number of A molecules within the receiver volume (due to a single emission of molecules) is found by integrating (2) over V_{obs}, which in spherical coordinates means

$$\overline{N_{A_0}}(t; t_0) = \int_0^{r_{\text{obs}}} \int_0^{2\pi} \int_0^{\pi} C_A(\vec{r}, t; t_0) r^2 \sin\theta\,\mathrm{d}\theta\,\mathrm{d}\phi\,\mathrm{d}r. \tag{4}$$

This integral can be simplified by utilizing the uniform concentration assumption [24], which states that the expected concentration throughout the receiver is equal to that expected at the center of the receiver, leading to

$$\overline{N_{A_0}}(t; t_0) = V_{\text{obs}} C_A(\vec{r}_{\text{eff}}, t; t_0), \tag{5}$$

where $V_{\text{obs}} = 4\pi r_{\text{obs}}^3/3$ and

$$|\vec{r}_{\text{eff}}(t)|^2 = \left(x_0 - \int_{t_0}^{t} v_x(\tau)\,\mathrm{d}\tau\right)^2 + \left(\int_{t_0}^{t} v_y(\tau)\,\mathrm{d}\tau\right)^2 + \left(\int_{t_0}^{t} v_z(\tau)\,\mathrm{d}\tau\right)^2 \tag{6}$$

is the square of the effective distance between the transmitter and the center of the receiver at $\vec{0}$, derived by setting $\vec{x} = \vec{0}$ in (3).

The statistics of the general receiver signal $N_{A_{\text{obs}}}(t)$ can be derived based on $\overline{N_{A_0}}(t; t_0)$ and the transmitted binary sequence $\mathbf{W}$, yielding the number of observed molecules due to sequential transmissions from the transmitter and noise. Assuming that A molecules diffuse randomly and independently, $N_{A_{\text{obs}}}(t)$ is a sum of time-varying Poisson random variables, as shown in [25], with time-varying mean

$$\overline{N_{A_{\text{obs}}}}(t) = \overline{N_{A_{\text{TX}}}}(t) + \overline{N_{A_n}}(t). \tag{7}$$

Here, $\overline{N_{A_n}}(t)$ is the mean number of molecules from the noise sources, and $\overline{N_{A_{\text{TX}}}}(t)$ is the mean number of observed molecules due to sequential emissions by the transmitter, i.e.,

$$\overline{N_{A_{\text{TX}}}}(t) = \sum_{j=1}^{\lfloor\frac{t}{T_{\text{int}}}+1\rfloor} W[j]\overline{N_{A_0}}\left(t; (j-1)T_{\text{int}}\right). \tag{8}$$

2.3. Weighted Sum Detectors

The detector relies on a common sampling scheme, where the receiver makes M observations in every bit interval. The value of the mth observation in the jth bit interval is labeled $s_{j,m}$. We define the sampling times within a single interval as the function $g(m)$, and the global time sampling function $t(j,m) = jT_{\text{int}} + g(m)$, where $j = \{1, 2, \ldots, B\}$ and $m = \{1, 2, \ldots, M\}$. In this work, we set $g(m) = mt_s$, implying that the observations are taken at times separated by constant period t_s. In addition, we assume that the transmitter and receiver are perfectly synchronized; that is, the transmitter knows the exact time that it has to inject the molecules into the channel, and the receiver detector knows the exact time that it has to sample.

We use the weighted sum detector proposed in [12] whose decision rule in the jth bit interval can be described as

$$\hat{W}[j] = \begin{cases} 1 & \text{if } \sum_{m=1}^{M} \omega_m N_{A_{\text{obs}}}(t(j,m)) \geq \gamma, \\ 0 & \text{otherwise,} \end{cases} \tag{9}$$

where ω_m is the weight of the mth observation and γ is the binary decision threshold. In this work, we set $\omega_m = \overline{N_{A_{\text{obs}}}}(g(m))$. In Ref. [12], it is analytically verified that the matched filter of setting the sample weight ω_m equal to the mean number of observed molecules $\overline{N_{A_{\text{obs}}}}(g(m))$ in (7) is optimal in the sense that it maximizes the signal-to-noise ratio and minimizes the bit error rate (BER) if the desired signal is corrupted by additive white Gaussian noise. However, channel noise in this work is characterised with a Poisson random variable, which means that the matched filter is not necessarily optimal. Even so, the simplicity of the weighted sum detector, compared to the optimal maximum likelihood detector [26], is desirable for practicalities of implementation and given that individual transceivers in MC systems generally have limited computational abilities and memory. An optimal γ can be acquired via numerical search [12].

3. Time-Varying Electric Fields

This section investigates two different time-varying (sinusoidal and optimized) electric fields to improve BER performance in MC systems. Bit decoding errors are generally reduced by increasing the signal strength (i.e., the number of observed molecules at the receiver site) and reducing the ISI between bit intervals (i.e., the number of residual molecules). Therefore, this section explores a method that exploits time-varying electric fields to maintain a high density of the information-carrying molecules within the receiver during the corresponding bit interval (to increase the signal strength) and migrate the molecules away from the receiver sphere just before the subsequent bit interval (to reduce the ISI).

3.1. Sinusoidal Field

In this section, we consider a sinusoidal electric field, which can be accurately generated and controlled even in small-sized and low-powered LoC applications [27]. Since $\vec{v}(t) \propto \vec{E}(t)$, we can express the induced sinusoidal molecule velocity (in m/s) as

$$\vec{v}(t) = \left\{ A_v \sin(2\pi f_v t - \phi_v) + \text{DC}_v, 0, 0 \right\}, \tag{10}$$

where A_v, f_v, ϕ_v, DC_v are the sinusoidal field's amplitude, frequency, phase shift and constant velocity offset, respectively. Without loss of generality, we assume that only x-axis flow exists (so the only non-zero component of $\vec{v}(t)$ is v_x), since the transmitter and receiver are aligned with the x-axis.

According to (2), the degree of dispersion of the molecules depends on the diffusion coefficient D_A and the time elapsed from being emitted by the transmitter, $t - t_0$. Since D_A is constant for a given fluid medium, we reduce the degree of molecule dispersion by reducing the time elapsed from emission. But as the expected number of observed molecules $\overline{N_{A_{\mathrm{obs}}}}(t)$ is inversely proportional to the degree of the molecules' dispersion at the receiver site, it would be wise to induce a time-varying electric field that sends the molecules toward the receiver as fast as possible immediately after they are emitted. This electric field strategy would allow the molecules to reach the receiver sphere with a higher density. Besides, to allow the detection mechanism described in Section 2.3 to sample as many molecules as possible (when a binary 1 is transmitted), the time-varying electric field must ensure that the molecules dwell inside the receiver sphere as long as possible once they arrive there. The time-varying electric field should then migrate the molecules away from the receiver sphere just before the next bit interval to reduce the ISI.

Based on this physical mechanism, we provide a method to find rational parameters for the sinusoidal field (A_v, DC_v, f_v, and ϕ_v) in terms of the induced sinusoidal velocity (10). First, setting $f_v = 1/T_{\mathrm{int}}$ is a natural choice to have a single velocity fluctuation in a single bit interval since we need to move the molecules twice quickly (towards and away from the receiver sphere) and once slowly (within the receiver sphere). We also constrain the mean square of the velocity[1] to conserve energy, which leads to

$$\frac{1}{T_{\mathrm{int}}} \int_0^{T_{\mathrm{int}}} \left(A_v \sin\left(2\pi(1/T_{\mathrm{int}})t - \phi_v\right) + \mathrm{DC}_v \right)^2 \mathrm{d}t \le \xi_v, \tag{11}$$

where ξ_v is the constraint value. It is necessary to maximize A_v to let the sinusoidal velocity retain the largest gap between its maximum and minimum peak values. This setup enables the molecule group to be quickly sent towards the receiver and ensures that its center stays within the receiver sphere for a long time. Since destructive flows, defined as a flow component not in the direction of transmission (i.e., a negative velocity), generally reduce the peak number of molecules expected to be observed at the receiver [22], we constrain the non-zero sinusoidal velocity component to be positive. Thus, by setting $A_v = \mathrm{DC}_v$, A_v and DC_v can be calculated from (11) as

$$A_v = \mathrm{DC}_v = \sqrt{\frac{2}{3}\xi_v}. \tag{12}$$

Regarding ϕ_v, in order to retain the center of the molecule group within the receiver sphere for as long as possible, the time that the induced velocity has a minimum should coincide with the time that the center of the molecule group reaches the center of the

---

[1]Note that this constraint is identical to constrain the average power of electric field since $\vec{v}(t) \propto \vec{E}(t)$.

receiver sphere. This criterion can be expressed as

$$\int_0^{t_1} \left(A_v \sin\left(2\pi f_v t - \phi_v\right) + \mathrm{DC}_v\right) \mathrm{d}t = x_0. \tag{13}$$

Here, t_1 should meet the conditions

$$v_x'(t_1) = 2\pi A_v f_v \cos\left(2\pi f_v t_1 - \phi_v\right) = 0 \text{ and}$$
$$v_x''(t_1) = -4\pi^2 A_v^2 f_v^2 \sin\left(2\pi f_v t_1 - \phi_v\right) > 0$$
$$\implies t_1 = \frac{1}{2\pi f_v}\left(\frac{3}{2}\pi + 2\pi n + \phi_v\right) \text{ for } n \in \mathbb{Z}, \tag{14}$$

where $\mathbb{Z}$ denotes the set of all integers. After substituting (14) into (13), we can numerically find ϕ_v satisfying the condition (13). Note that the method explained above is not proved optimal. However, as will be shown in Section 5, the induced sinusoidal velocity obtained via this method significantly increases the expected number of observed molecules at the receiver, compared to the constant electric field benchmark.

Fig. 2 illustrates how time-varying sinusoidal electric fields move molecules throughout a bit interval. The center of the molecule group emitted at $t = 0$ is shown according to the time elapsed, both when a sinusoidal electric field (two phases, $\phi_v = 5.07$ and π (rad)) and a constant electric field are applied. The values on the vertical axis of the figures are calculated as $\int_0^t v_x(\tau)\,\mathrm{d}\tau$. For the sinusoidal electric field in Fig. 2(a), $v_x(t) = 8.17\times 10^{-3}\sin(2\pi\times 10^4 t - 5.07) + 8.17\times 10^{-3}$ (m/s) is obtained from the criterion (13), while the sinusoidal field with $\phi_v = \pi$ (rad) in Fig. 2(b) is given as a benchmark, along with the constant induced velocity $v_x(t) = 0.01$ (m/s) in Fig. 2(c). All of the velocities have the same average power, 10^{-4}. In addition, the standard deviation of the molecules' distribution from the center of the molecule group, $\sigma_x = \sqrt{2D_A t}$, is shaded. Note that the transmitter and the receiver sphere are located at $\{-x_0, 0, 0\}$ and $\{0, 0, 0\}$, respectively; thus, the distance between the transmitter and receiver is x_0 ($= 0.5\,\mu\mathrm{m}$ in the figure). The receiver sphere region (spanning $2r_{\mathrm{obs}}$ along the x-axis) is delineated by the two dashed horizontal lines. All other system parameters are given in Table 1.

In Fig. 2(a), the center of the molecule group (the solid blue line) quickly reaches the receiver sphere and remains within the receiver sphere region for a long time. In contrast, in Fig. 2(b) and (c) the molecule group slowly reaches, and quickly passes through, the receiver sphere. Moreover, the degree of molecule dispersion in Fig. 2(a) when the center of the molecule group reaches the receiver sphere (vertical span of the shaded region) is smaller than that in either Fig. 2(b) or (c). Note that the molecules' standard deviation from the center of the molecule group is proportional to the elapsed time t. Since the density of molecules at the receiver site in Fig. 2(a) is higher, the expected number of observed molecules $\overline{N_{A_{\mathrm{obs}}}}(t)$ when the center of the molecule group is within the receiver sphere is also higher than those of Fig. 2(b) and (c). Besides, for the sampling scheme described in Section 2.3, which makes multiple observations at times separated by a constant interval, an increase in the duration that the molecules dwell in the receiver sphere increases the value of the weighted sum in (9) (when a binary 1 is transmitted). These features of the sinusoidal electric field with phase $\phi_v = 5.07$, shown in Fig. 2(a),
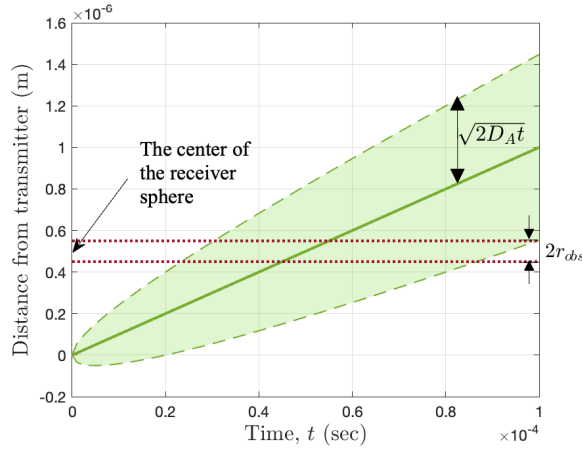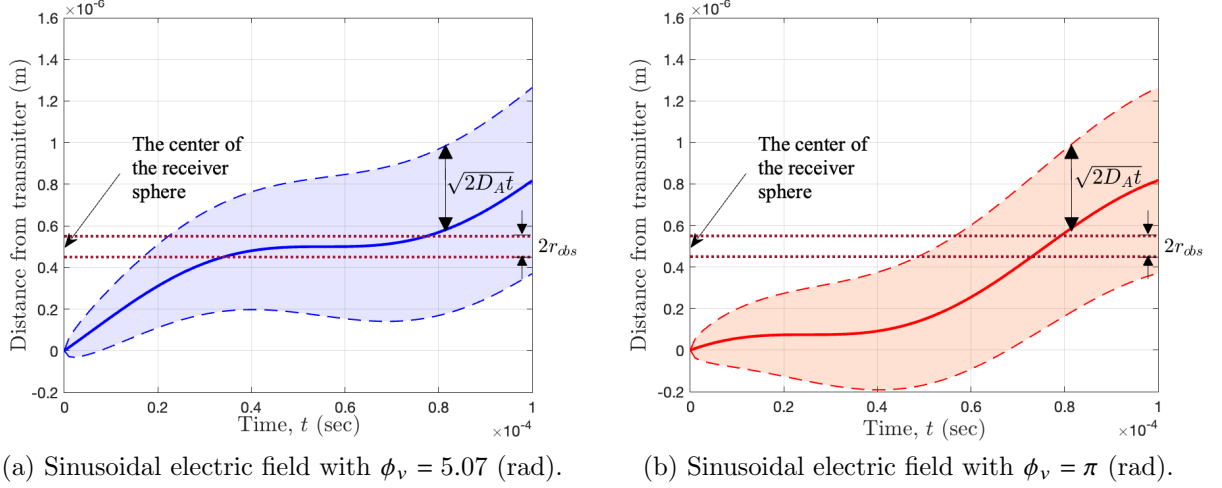
9

(a) Sinusoidal electric field with $\phi_v = 5.07$ (rad).

(b) Sinusoidal electric field with $\phi_v = \pi$ (rad).

(c) Constant electric field, with $v_x(t) = 0.01$ (m/s).

Figure 2. The temporal position of the center of the molecule group, resulting from two sinusoidal electric fields (with the different phases ϕ_v) and a constant electric field benchmark. The sinusoidal velocity parameters $A_v = 8.17 \times 10^{-3}$, $f_v = 10^4$ (Hz), and $DC_v = 8.17 \times 10^{-3}$ are used, while $\phi_v = 5.07$ and π (rad) are differently used in panels (a) and (b), respectively. The constant field $v_x(t) = 0.01$ (m/s) is used in panel (c). Other system parameters are provided in Table 1 in Section 5.

significantly improve the bit error performance compared to the two comparison fields, as verified in Section 5.

3.2. Optimized Field

Further developing the advantages of the sinusoidal electric field discussed in Section 3.1, this section analytically derives an optimized electric field that colocates the center of the molecule group and the receiver sphere for as long as possible. First, we formulate a cost function of the mean squared error between the receiver's center and the center of the molecule group as

$$\text{Cost}[x, x'] = \frac{1}{T_{\text{int}}} \int_0^{T_{\text{int}}} (x(t) - x_0)^2 \, \mathrm{d}t \tag{15a}$$

10

$$\text{such that} \begin{cases} \dfrac{1}{T_{\text{int}}} \displaystyle\int_0^{T_{\text{int}}} v_x^2(t)\,dt \le \xi_v, \\ IC : x(0) = 0, \\ FC : x(T_{\text{int}}) = x_1, \end{cases} \tag{15b}$$

where $x(t) = \int_0^t v_x(\tau)\,d\tau$ denotes the distance between the center of the molecule group and the transmitter. Our goal is to minimize the cost function (15a), subject to the constraints in (15b). We solve this optimization problem under the framework of calculus of variations. The first constraint limits the average power of electric field, and the final condition FC is set in order to migrate the molecules in the current bit interval away for the new molecules coming in the next bit interval. In other words, setting $x_1 = x_0$ corresponds to the center of the molecule group being located at the center of the receiver sphere at the end of the bit interval, and setting $x_1 > x_0$ corresponds to the center of the molecule group passing the receiver. In real systems, conditioning would be according to the requirements of the device, e.g., the location of transducer/biosensor outlets in LoC devices.

Letting $x'(t) = v_x(t)$, we form the Lagrangian

$$\mathcal{L}[x(t), x'(t)] = [x(t) - x_0]^2 + \mu\, [x'(t)]^2, \tag{16}$$

where $\mu \in \mathbb{R}$ is the Lagrange multiplier. Therefore, the Euler-Lagrange equation [28] can be written as

$$\frac{d}{dt}\left(\frac{\partial \mathcal{L}}{\partial x'(t)}\right) - \frac{\partial \mathcal{L}}{\partial x(t)} = \frac{d}{dt}\left(2\mu x'(t)\right) - 2\left(x(t) - x_0\right) = 0. \tag{17}$$

Letting $y(t) = x(t) - x_0$, so $y'(t) = x'(t)$, we can rewrite (17) as

$$y''(t) - \lambda^2 y(t) = 0, \tag{18}$$

where $\mu = 1/\lambda^2$. Therefore, we can obtain the stationary path $x(t)$ as

$$x^\star(t) = C_1 e^{\lambda t} + C_2 e^{-\lambda t} + x_0, \tag{19}$$

where C_1 and C_2 are obtained by utilizing the initial and final conditions (IC and FC) in (15b), i.e., $x^\star(0) = C_1 + C_2 + x_0 = 0$ and $x^\star(T_{\text{int}}) = C_1 e^{\lambda T_{\text{int}}} + C_2 e^{-\lambda T_{\text{int}}} + x_0 = x_1$, respectively, with

$$C_1 = \frac{(1 - e^{-T_{\text{int}}\lambda})x_0 - x_1}{e^{-T_{\text{int}}\lambda} - e^{T_{\text{int}}\lambda}} \quad \text{and} \tag{20a}$$

$$C_2 = -x_0 - \frac{(1 - e^{-T_{\text{int}}\lambda})x_0 - x_1}{e^{-T_{\text{int}}\lambda} - e^{T_{\text{int}}\lambda}}. \tag{20b}$$

λ can be numerically found from evaluating the integral of the first constraint in (15b) as

$$\frac{\lambda}{2T_{\text{int}}}\left[C_1^2(e^{2T_{\text{int}}\lambda} - 1) + C_2^2(-e^{-2T_{\text{int}}\lambda} + 1) - 4C_1 C_2 T_{\text{int}}\lambda\right] = \xi_v. \tag{21}$$

11

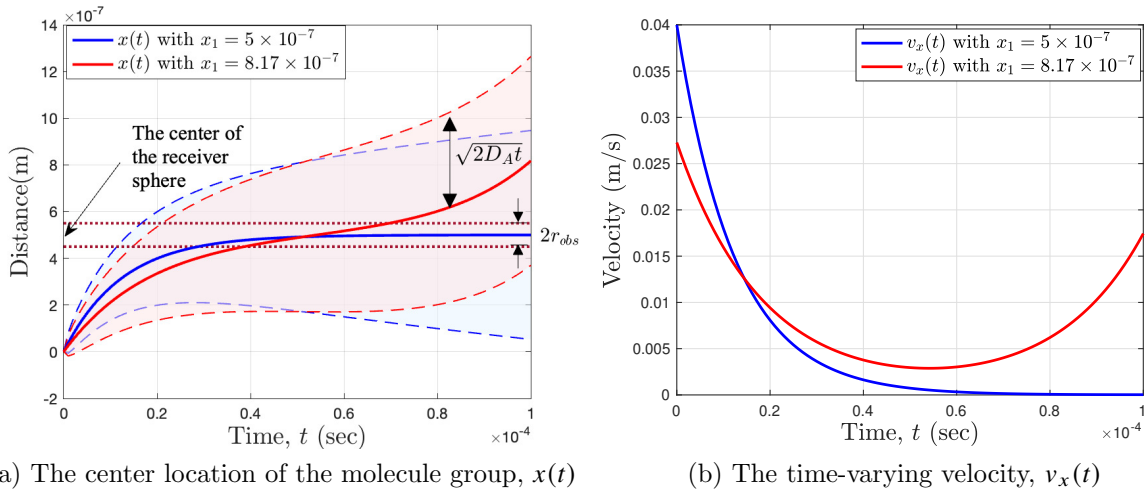(a) The center location of the molecule group, $x(t)$ (b) The time-varying velocity, $v_x(t)$

Figure 3. The location of the center of the molecule group and the x-axis velocity $v_x(t)$ of the molecules according to the elapsed time, when the optimized electric field is applied (with velocity obtained from (15)). $\xi_v = 10^{-4}$ is assumed. Other system parameters are provided in Table 1.

One can study the second variation of the problem to ascertain whether the stationary path yields a minimum value of the functional; however, it is clear that the stationary path $x^\star$ in (19) yields a minimum because of the problem formulation, i.e., the quadratic cost function subject to the constraints. Finally, the velocity induced by the optimized electric field can be obtained as

$$v_x^\star(t) = (x^\star(t))' = C_1 \lambda e^{\lambda t} - C_2 \lambda e^{-\lambda t} \quad (\mathrm{m\,s^{-1}}), \tag{22}$$

which has a form of exponential functions.

Fig. 3 illustrates the location of the center of the molecule group and the x-axis velocity of the molecule flow according to the elapsed time when the optimized electric field (15) is employed with the different final conditions x_1. The bit time interval $T_{\mathrm{int}} = 10^{-4}$ (sec) is used. Note that the final condition $x_1 = 8.17 \times 10^{-7}$ (m) is identical to the travel distance of the center of the molecule group in a single bit interval with the sinusoidal velocity in Figs. 2(a) and (b), whilst $x_1 = 5 \times 10^{-7}$ coincides with the location of the receiver. From the figures, we can note that the optimized field initially propagates the molecules at high speed immediately after emission, then rapidly reduces their speed to ensure that the molecules remain at the receiver sphere for a long time. Just before the next bit interval, the velocity is increased to migrate the molecules away, which mitigates ISI (when the final condition is $x_1 > x_0$).

4. Balance Between Electrophoretic and Viscous Forces

In previous sections, we assumed that the electrophoretic force $\vec{F}_E(t) = q_A \vec{E}(t)$ induces molecular motion with velocity $\vec{v}(t)$ via a linear relation, $\vec{E}(t) \propto \vec{v}(t)$. However, the actual molecule velocity $\vec{u}(t)$ may not necessarily be linearly related to the electric field, as assumed to obtain $\vec{v}(t)$, due to a viscous drag force and an added mass effect, especially

12

during the period of initial acceleration following emission that is implied by both the sinusoidal and optimized fields from Section 3. In other words, $\vec{v}(t)$ can be interpreted as the one that we intend to generate using the electrophoretic force $\vec{F}_E(t)$, while $\vec{u}(t)$ is the actual velocity achieved, notwithstanding fluid dynamic effects. Therefore, in this section, we derive and analytically solve an ordinary differential equation (ODE) for the time-varying sinusoidal and exponential electric fields to determine when $\vec{u}(t) \approx \vec{v}(t)$ for $t \neq 0$ is satisfied.

In fluid dynamics, the Basset–Boussinesq–Oseen (BBO) ODE describes the motion of – and forces on – a small particle/molecule in unsteady flow at low Reynolds number [29]. This equation considers 1) the viscous drag, 2) the added mass effect, 3) the pressure gradient force due to an unsteady undisturbed flow, 4) the Basset force (a history force due to the non-instantaneous molecule boundary layer development), and 5) other body forces, such as the electrophoretic force and gravity. First, the viscous drag for a spherical molecule is given by Stokes' law as $F_D(t) = c_d \vec{u}(t)$ in the limit of a small Reynolds number, where $c_d = 6\pi\mu_f r_m$ is the frictional drag coefficient, μ_f is the dynamic viscosity of the fluid, and r_m is the molecule radius. Second, the added mass effect arises due to the displacement of fluid required to accelerate the molecule through the ambient fluid [29]. For a spherical molecule, the added mass comprises a fluid region of half the molecule volume. Moreover, we assume an undisturbed flow (i.e. zero pressure gradient force) and neglect gravity due to the small molecule size. We also neglect the Basset force, which is a common assumption in the literature for conceptual simplicity and flow considerations [30, 31]. The assumptions made here are reviewed in Section 6.

Based on these assumptions, we formulate a first-order BBO ODE as

$$\frac{2}{3}\pi r_m^3 (2\rho_m + \rho_f)\frac{\mathrm{d}\vec{u}(t)}{\mathrm{d}t} + 6\pi\mu_f r_m \vec{u}(t) = q_A \vec{E}(t), \tag{23}$$

where ρ_m and ρ_f are the molecule and fluid densities, respectively [30]. We consider a *single* molecule introduced at $t = 0$ with zero velocity; thus, the initial condition is $\vec{u}(0) = \vec{0}$. Building on the assumption that the electric field $\vec{E}(t)$ is linearly related to the molecule velocity $\vec{v}(t)$, we set $\vec{E}(t) = (c_d/q_A)\vec{v}(t)$ and plug this into (23). Here, $\vec{v}(t)$ is interpreted as the *desired* velocity of the molecule (that we want the molecule to achieve), and $\vec{E}(t)$ is the *applied* electric field required to induce the desired velocity $\vec{v}(t)$. In other words, by solving the ODE (23) for $\vec{u}(t)$, we can investigate the difference between the instantaneous molecule velocity $\vec{u}(t)$ induced when $\vec{E}(t)$ is applied, and the desired molecule velocity $\vec{v}(t)$.

Note that the left side of (23) can be divided into mass (first) and viscous (second) terms. To make $\vec{u}(t) \approx \vec{v}(t)$, the viscous term must dominate the mass term throughout the dynamics so that $6\pi\mu_f r_m \vec{u}(t) \approx c_d \vec{v}(t)$ (recall that $c_d = 6\pi\mu_f r_m$), when $\vec{v}$ is not close to zero. This condition can be expressed as

$$\frac{2}{3}\pi r_m^3 (2\rho_m + \rho_f)\left|\frac{\mathrm{d}\vec{u}(t)}{\mathrm{d}t}\right| \ll 6\pi\mu_f r_m |\vec{u}(t)|, \tag{24}$$
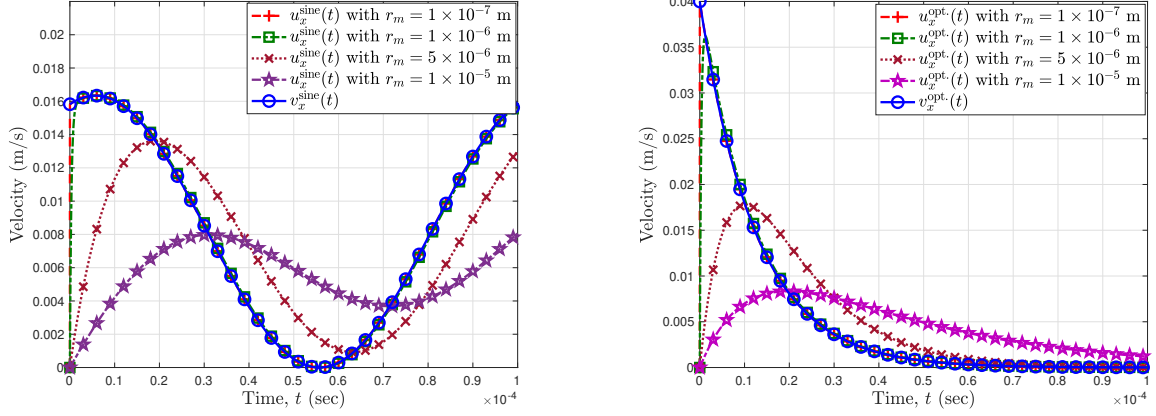
(a) $v_x^{\text{sine}}(t) = 8.17 \times 10^{-3} \sin(2\pi \times 10^4 t - 5.07) + 8.17 \times 10^{-3}$ (m/s) and its corresponding $u_x^{\text{sine}}(t)$ in (26) are used.

(b) $v_x^{\text{opt.}}(t) = 0.04 e^{-80000t}$ (m/s) and its corresponding $u_x^{\text{opt.}}(t)$ in (27) are used.

Figure 4. Comparison between instantaneous velocities $u_x(t)$ (accounting for mass and viscosity) for different molecule radii and the desired velocity $v_x(t)$. The sinusoidal and optimized fields from Fig. 2(a) and Fig. 3(b) are assumed in (a) and (b), respectively.

which provides the feasible region for the particle radius r_m as

$$ r_m \ll \sqrt{\frac{9\mu_f |\vec{u}(t)|}{(2\rho_m + \rho_f) \, |\mathrm{d}\vec{u}(t)/\mathrm{d}t|}}. \tag{25} $$

We now consider two examples based on the time-varying electric fields studied in Section 3 to elucidate (25). We assume flow only in the x direction, so only the corresponding vector component appears here. For the sinusoidal field, (23) can be integrated (using (10)) to

$$ \begin{aligned} u_x^{\text{sine}}(t) = {} & \frac{c_d \Omega}{\Gamma} \sin(2\pi f_v t - \phi_v) - 2\pi f_v \Omega \cos(2\pi f_v t - \phi_v) + DC_v \\ & + \left[\frac{c_d \Omega}{\Gamma} \sin(\phi_v) + 2\pi f_v \Omega \cos(\phi_v) - DC_v \right] \exp\left(-\frac{c_d t}{\Gamma}\right), \end{aligned} \tag{26} $$

where

$$ \Omega = \frac{\Gamma A_v c_d}{c_d^2 + (2\pi f_v \Gamma)^2} \quad \text{and} \quad \Gamma = \frac{2}{3}\pi r_m^3 (2\rho_m + \rho_f). $$

Employing the sinusoidal velocity parameters as used in Fig. 2(a), and the environment parameters $\rho_m = \rho_f = 10^3$ kg m^{-3} and $\mu_f = 10^{-3}$ Pa s, $u_x^{\text{sine}}(t)$ is plotted over a single bit interval time for different values of r_m in Fig. 4(a). $v_x^{\text{sine}}(t)$ is also plotted for comparison.

For the optimized field introduced in Section 3.2 with the final condition $x_1 = x_0$ (i.e., $C_1 = 0$), (23) can be integrated to obtain

$$ u_x^{\text{opt.}}(t) = \frac{\lambda c_d C_2}{c_d - \lambda \Gamma} \left[\exp(-c_d t / \Gamma) - \exp(-\lambda t) \right], \tag{27} $$

with $v_x^{\text{opt.}}(t)$ given by (22). Using the parameters from Fig. 3(b), namely $C_2 = -5 \times 10^{-7}$

14

and $\lambda = 8 \times 10^4$, $u_x^{\text{opt.}}(t)$ is plotted for different values of r_m, alongside $v_x^{\text{opt.}}(t)$, in Fig. 4(b).

For both cases in Figs. 4(a) and (b), $u_x(t)$ for $r_m \lesssim 1 \times 10^{-6}$ m shows insignificant deviation from $v_x(t)$, verifying that the applied electric field can linearly induce the molecule velocity $\vec{v}$ for such small molecule sizes. For $r_m = 1 \times 10^{-6}$ m, although there is a degree of deviation between $u_x(t)$ and $v_x(t)$ during the initial acceleration of the former, the instantaneous velocity grows quickly enough that the deviation becomes negligible after only a few microseconds. However, for larger molecule radii (notably $r_m = 5 \times 10^{-6}$ m and 1×10^{-5} m), a persistent lag between $u_x(t)$ and $v_x(t)$ exists, which shows that the electric field cannot linearly produce the desired molecule velocity when the molecule radius is not sufficiently small.

The main implication of Fig. 4 is that for $\vec{u}(t) \approx \vec{v}(t)$, $\vec{u}(t)$ must grow sufficiently quickly from 0 m/s at $t = 0$ to catch up $\vec{v}(t)$ that is not zero at $t = 0$. We can relate this requirement to (25). For example, with the sinusoidal electric field ($\phi_v = 5.07$) considered above, (25) is first satisfied (taken here to mean that the right-hand side is at least 10 times bigger than the left-hand side) within 1.7% of the bit interval when $r_m = 1 \times 10^{-6}$ m, whereas 18.7% of the bit interval is required for $r_m = 5 \times 10^{-6}$ m to satisfy (25). Hence, in the former case the viscous term quickly dominates the mass term after $t = 0$, but not in the latter case, which explains the deviation seen between $u_x(t)$ and $v_x(t)$ in Fig. 4(a) when $r_m = 5 \times 10^{-6}$ m. Similar conclusions can be drawn for the optimized electric field displayed in Fig. 4(b).

For the system model considered in this work (see Table 1), the diffusion coefficient $D_A = 10^{-9}$ m^2 s^{-1} implies a molecule radius of $r_m = 2.2 \times 10^{-10}$ m with a room temperature environment, via the Stokes-Einstein equation. Based on the above analysis, this implied radius is several orders of magnitudes lower than those for which the viscous term looses its dominance, indicating that the proposed electrophoretic MC framework is feasible from a fluid dynamics perspective. Hence, under the conditions in which molecules' radii are adequately small, and in particular throughout all other sections of this work, we can reliably say that $\vec{u}(t) \approx \vec{v}(t)$ for $t \neq 0$ and assume equivalency between the magnitudes of $\vec{E}(t)$ and $\vec{v}(t)$.

5. Numerical results

In this section, we provide numerical results to verify our analysis in Section 3. The system parameters are provided in Table 1. Note that $\xi = 10^{-4}$ is chosen such that the optimal field and the constant field inducing $v_x(t) = 0.01$ m/s have the same average power. The simulation results were obtained via a Monte Carlo approach with 10^4 trials. In the simulations, we generate Poisson random variables with the time-varying mean $\overline{N_{A_{\text{obs}}}}(jT_{\text{int}} + g(m))$ to mimic the observation value $s_{j,m}$, and estimate the transmitted binary sequence $\mathbf{W}$ based on the generated values of $s_{j,m}$ by using the weighted sum detector (9). The BER is subsequently calculated. This approach can be justified by the fact that $s_{j,m}$ is approximated well by the Poisson random variables with time-varying mean [12]. Note that the independence between adjacent observations becomes negligible as the sampling interval t_s increases. This simulation approach significantly reduces the computational cost compared to a microscopic simulation approach.

Table 1. System parameters, adopted from [22].

Parameter	Symbol	Value
Number of molecules per emission	N_{EM}	10^4
Probability of binary 1	P_1	0.5
Length of transmitter sequence	B	100 bits
Bit interval time	T_{int}	0.1 ms
Diffusion coefficient	D_A	$10^{-9}\ \mathrm{m^2\,s^{-1}}$
Location of transmitter	x_0	$0.5\,\mu\mathrm{m}$
Radius of receiver	r_{obs}	$50\,\mathrm{nm}$
Expected impact of noise source(s)	$\overline{N_{A_n}}(t)$	1 molecule
Number of samples at detector	M	5
Average power constraint	ξ_v	10^{-4}

Fig. 5 shows the expected number of observed molecules within the receiver volume $\overline{N_{A_{\mathrm{obs}}}}(t)$ and the x-axis velocity component $v_x(t)$ when different electric fields are employed. The assumed transmitted binary sequences are fixed as $\{1, 0, 1, 0, 0, 1, 0, \ldots\}$ for all the cases; only the first 7 bits are illustrated in the figures. Note that the optimized electric field, with the final condition $x_1 = x_0 = 5 \times 10^{-7}$, yields the highest expected number of observed molecules, while the constant field leads to the lowest number. It is also shown that the number of the residual molecules in the next time slot (i.e., the ISI) is highest under the optimized electric field (see the region of $0.3 \sim 0.4 \times 10^{-3}$ (sec)), which might adversely affect the BER performance. However, the fact that the BER result of $\{0.10, 0.27, 0.75, 1.80\} \times 10^{-2}$ for each velocity improves (decreases) as the expected number of observed molecules increases verifies that increasing the number of observed molecules (i.e. propagation efficiency) is more important for reducing bit errors than reducing the ISI with the considered detection scheme. Note that the derived electric field is optimized with respect to reducing the mean squared error in (15a), rather than minimizing the ISI; however, the level of ISI can be changed by manipulating the final condition x_1 in (15b) if required.

Fig. 6(a) shows the BER performance for the different bit interval times T_{int}. In conventional wireless or wired communications, when T_{int} increases, it is expected that ISI would decrease, so that the BER would also decrease. However, Fig. 6 demonstrates that the BER increases as T_{int} increases for both the sinusoidal and optimized electric fields. Although ISI between the bit intervals can decrease with increased bit interval time, the molecules can also diffuse more widely. Thus, the expected number of observed molecules over a single bit interval decreases, and the BER consequently worsens. In contrast, since the optimized electric field quickly propagates the molecules and ensures that the center of the molecule group stays within the receiver sphere for a long time, its BER can reduce as T_{int} increases.

Fig. 6(b) shows the BER performance for the different average power constraints ξ_v. The BER performance curve is not monotonic when the constant field is employed. Since this work employs a constant sampling time t_s as described in Section 2.3, the BER performance appears good when the center of the molecule group passes through the receiver sphere at the times that the observations are taken, i.e. $jT_{\mathrm{int}} + m\,(T_{\mathrm{int}}/M)$, where
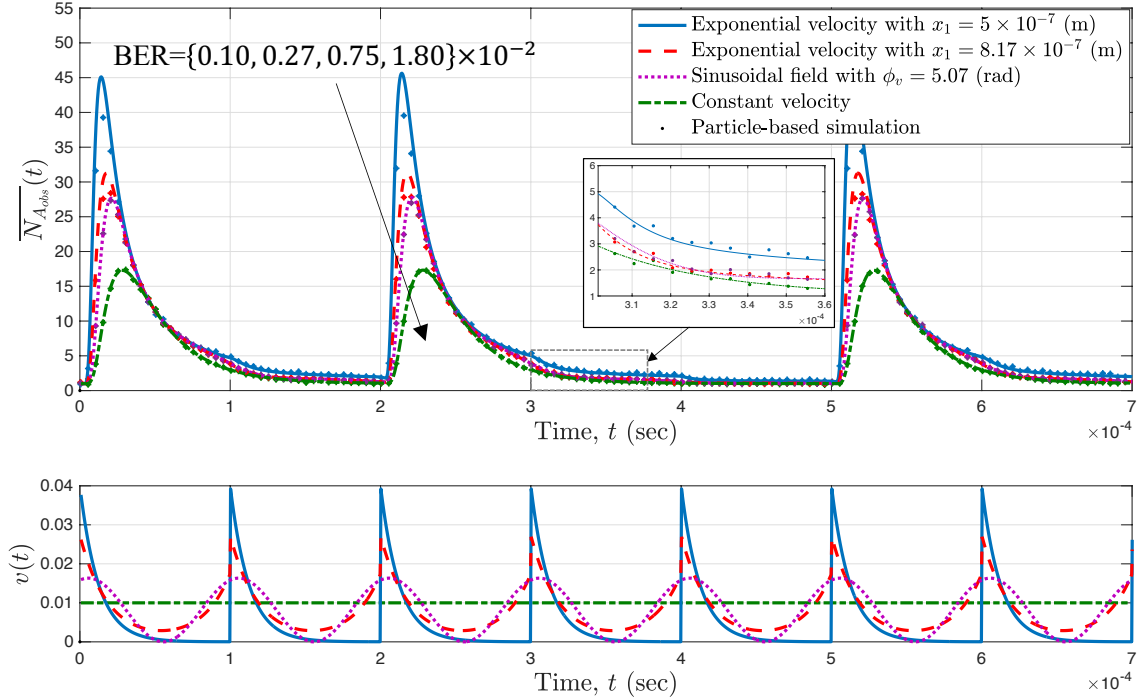
Figure 5. The expected number of molecules observed within the receiver volume $\overline{N_{A_{\mathrm{obs}}}}(t)$ for the different types of electric field, and therefore molecule velocities $v_x(t)$. The solid lines are obtained from numerically evaluating (7), while the dotted lines are obtained by averaging over 10^3 independent particle-based simulation trials.

$j = \{1, 2, \ldots, B\}$, $m = \{1, 2, \ldots, M\}$. In contrast, the BER performance worsens when the crossing time of the center of the molecules group and the receiver sphere deviates from the sampling points. In other words, the BER performance for a constant electric field is dependent on the sampling time, which must be taken into account in engineered MC systems with advection. In contrast, when the sinusoidal and optimized electric fields are employed, it is shown that the BER performance improves as the allowed average power ξ_v increases, independent of the sampling time. This improvement in performance is because these fields propagate the center of the molecule group toward the receiver site more quickly, and make it remain for longer within the receiver sphere as ξ_v increases.

Fig. 6(c) shows the BER performance for different numbers of samples per bit interval M. As the number of samples increases, the BER performance for all fields improves. This effect arises because the probability that the observations are taken when the centre of the molecule group is close to the center of the receiver sphere rises with larger M; thus, the weighted sum in (9) (when a binary 1 is transmitted) also increases, which results in a lower BER.

6. Discussion

The work presented here constitutes a theoretical basis for using time-varying electric fields to controllably propagate charged molecules via electrophoresis in MC systems, which we showed can improve communication performance. In order to concentrate on the utility of the proposed framework, in previous sections we considered an idealized
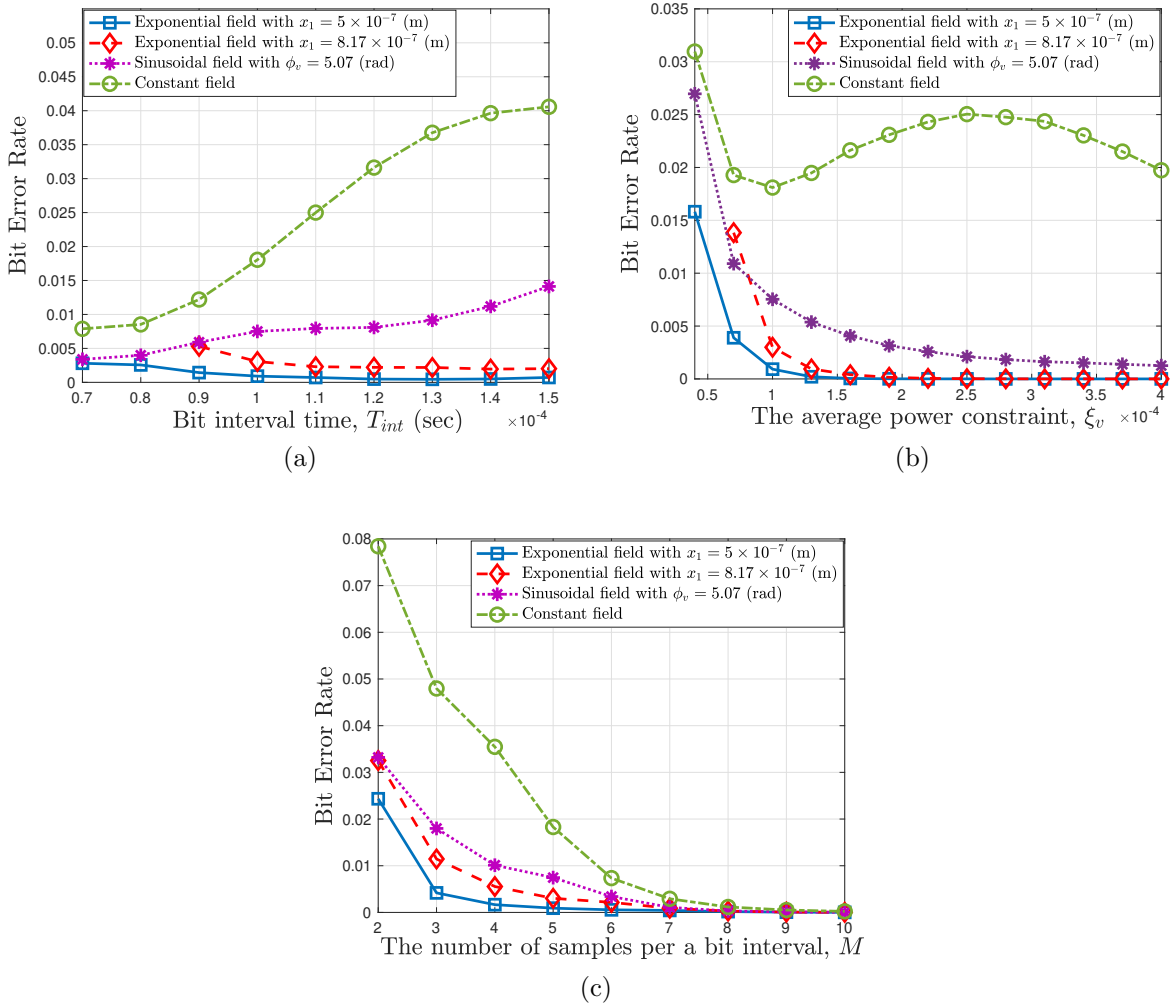
Figure 6. BER for different system parameters.

MC system with various assumptions to reduce the communication model's complexity. Given our positive results, further research is desirable to quantify the effects of some of our assumptions and to incorporate the proposed framework in real nanonetworks.

A key assumption made here is an infinite fluid environment. The flows in the LoC applications of particular interest are confined in bounded channels, which act to constrain the information-carrying molecules, significantly influencing the receiver signal model. There may also be specific wall effects. In particular, bounded channels may see an increase the ISI between bit intervals because previously transmitted molecules would not diffuse away to infinity. MC in bounded channels with circular and rectangular cross-sections has been studied by various authors (e.g., Refs. [32–34]), though it would be essential and compelling future work to examine how bounded channels affect communication performance within the proposed electrophoretic MC framework.

Beyond the assumptions on the extent of the domain, we also assumed a point transmitter with an impulsive injection method that introduces many molecules (N_{EM}) at a single point in space and time. It is well known that a molecule's motion is influenced (hindered) by those around it, while the analysis of fluid dynamic feasibility in Section 4

considered a single isolated molecule for conceptual simplicity. Moreover, electrostatic repulsion between the like-charged molecules (essential for electrophoresis) will induce additional motion not accounted for here. We hypothesize two scenarios that could feasibly occur in such MC systems: 1) significant electrostatic repulsion, so the molecules effectively travel individually, where hindrance can be accounted for in (23) with an effective fluid viscosity [35]; 2) the molecules remain concentrated and travel towards the receiver as a larger collective (porous) particle. Either case will tighten the molecule radius constraint (25) for which $\vec{u}(t) \approx \vec{v}(t)$ (so the electric field can appropriately control the molecules' velocity), although the assumption is likely still to hold for typical molecule sizes $O(10^{-10})$ m of interest in MC applications – future research may constrain the molecule radius more precisely. Also neglected in (23) is the viscous molecule history effect (Basset force, as noted in Section 4), which may play a non-negligible role, especially for the optimized electric field due to its impulse-like manifestation in the molecule velocity [36], in addition to any non-sphericity of the molecules. These physical features concerning the point transmitter need to be considered for the proposed framework to be implemented in practice.

7. Conclusions

We studied electrophoretic molecular communication systems with a time-varying flow of information-carrying molecules to achieve enhanced communication performance. The advantages of the proposed electrophoretic system can be extended beyond the MC framework to developing and improving microfluidic device technologies. Sinusoidal and exponential time-varying electric fields were used to induce molecule flow. These were designed to position the molecules at the receiver site with a high density for as long as possible to maximize the probability of reception/detection. In this way, we were able to increase the expected number of observed molecules and improve the BER performance. Our work is based on the assumption that molecule velocity is proportional to the electric field strength. We verified this assumption with an analysis of the fluid dynamics of the system. Analytical and numerical results demonstrated the feasibility and efficacy of the proposed electrophoretic approach to achieving molecular communication. Given the compelling results from this investigation, future efforts will be focused on refining the model to confined propagation media with a view to exploring the suitability of these techniques in specific lab-on-a-chip applications.

References

[1] N. Farsad, H. B. Yilmaz, A. Eckford, C. Chae, W. Guo, A comprehensive survey of recent advancements in molecular communication, IEEE Commun. Surv. Tutorials 18 (3) (2016) 1887–1919. doi:10.1109/comst.2016.2527741.

[2] I. F. Akyildiz, F. Brunetti, C. Blázquez, Nanonetworks: A new communication paradigm, Comput. Netw. 52 (12) (2008) 2260–2279. doi:10.1016/j.comnet.2008.04.001.

[3] I. F. Akyildiz, J. M. Jornet, M. Pierobon, Nanonetworks: A new frontier in communications, Commun. ACM 54 (11) (2011) 84–89. doi:10.1145/2018396.2018417.

[4] G. Leef, S. M. Thomas, Molecular communication between tumor-associated fibroblasts and head and neck squamous cell carcinoma, Oral Oncol. 49 (5) (2013) 381–386. doi:10.1016/j.oraloncology.2012.12.014.

[5] M. Kuscu, E. Dinc, B. A. Bilgin, H. Ramezani, O. B. Akan, Transmitter and receiver architectures for molecular communications: A survey on physical design with modulation, coding, and detection techniques, Proc. IEEE 107 (7) (2019) 1302–1341. doi:10.1109/jproc.2019.2916081.

[6] S. Hiyama, Y. Moritani, Molecular communication: Harnessing biochemical materials to engineer biomimetic communication systems, Nano Commun. Networks 1 (1) (2010) 20–30. doi:10.1016/j.nancom.2010.04.003.

[7] N. Farsad, W. Guo, A. W. Eckford, Tabletop molecular communication: Text messages through chemical signals, PloS One 8 (12) (2013) 1–13. doi:10.1371/journal.pone.0082935.

[8] D. Bi, A. Almpanis, A. Noel, Y. Deng, R. Schober, A survey of molecular communication in cell biology: Establishing a new hierarchy for interdisciplinary applications, IEEE Commun. Surv. Tutorials (2021). doi:10.1109/comst.2021.3066117.

[9] S. Kadloor, R. S. Adve, A. W. Eckford, Molecular communication using brownian motion with drift, IEEE Trans. Nanobiosci. 11 (2) (2012) 89–99. doi:10.1109/tnb.2012.2190546.

[10] D. Miorandi, A stochastic model for molecular communications, Nano Commun. Netw. 2 (4) (2011) 205–212. doi:10.1016/j.nancom.2011.04.005.

[11] K. V. Srinivas, A. W. Eckford, R. S. Adve, Molecular communication in fluid media: The additive inverse gaussian noise channel, IEEE Trans. Inf. Theory 58 (7) (2012) 4678–4692. doi:10.1109/tit.2012.2193554.

[12] A. Noel, K. C. Cheung, R. Schober, Optimal receiver design for diffusive molecular communication with flow and additive noise, IEEE Trans. Nanobiosci. 13 (3) (2014) 350–362. doi:10.1109/tnb.2014.2337239.

[13] N. Kim, A. W. Eckford, C. Chae, Symbol interval optimization for molecular communication with drift, IEEE Trans. Nanobiosci. 13 (3) (2014) 223–229. doi:10.1109/tnb.2014.2342259.

[14] V. Jamali, N. Farsad, R. Schober, A. Goldsmith, Non-coherent detection for diffusive molecular communication systems, IEEE Trans. Commun. 66 (6) (2018) 2515–2531. doi:10.1109/tcomm.2018.2792457.

[15] I. F. Akyildiz, M. Pierobon, S. Balasubramaniam, An information theoretic framework to analyze molecular communication systems based on statistical mechanics, Proc. IEEE 107 (7) (2019) 1230–1255. doi:10.1109/jproc.2019.2927926.

[16] T. Voitsekhivska, E. Suthau, K. Wolter, CMOS multiplexer for portable biosensing system with integrated microfluidic interface, in: 2014 IEEE ECTC in Lake Buena Vista, Florida, USA, 2014, pp. 173–178. doi:10.1109/ectc.2014.6897285.

[17] P. Manocha, G. Chandwani, S. Das, Dielectrophoretic relay assisted molecular communication for in-sequence molecule delivery, IEEE Trans. Nanobiosci. 15 (7) (2016) 781–791. doi:10.1109/tnb.2016.2618904.

[18] P. Manocha, G. Chandwani, S. Das, Characterization of dielectrophoresis based relay-assisted molecular communication using analogue transmission line, IEEE Access 8 (2020) 33352–33359. doi:10.1109/access.2020.2974067.

[19] Y. Xu, Tutorial: Capillary electrophoresis, Chem. Educ. 1 (2) (1996) 1–14. doi:10.1007/s00897960023a.

[20] N. Abd Rahman, F. Ibrahim, B. Yafouz, Dielectrophoresis for biomedical sciences applications: A review, Sensors 17 (3) (2017) 449. doi:10.3390/s17030449.

[21] H. Sedgwick, F. Caron, P. B. Monaghan, W. Kolch, J. M. Cooper, Lab-on-a-chip technologies for proteomic analysis from isolated cells, J. R. Soc. Interface 5 (2008) S123–S130. doi:10.1098/rsif.2008.0169.focus.

[22] A. Noel, K. C. Cheung, R. Schober, Diffusive molecular communication with disruptive flows, in: 2014 IEEE ICC in Sydney, Australia, 2014, pp. 3600–3606. doi:10.1109/icc.2014.6883880.

[23] H. C. Berg, Random Walks in Biology, Princeton University Press, 2018. doi:10.1098/rsif.2008.0014.

[24] A. Noel, K. C. Cheung, R. Schober, Using dimensional analysis to assess scalability and accuracy in molecular communication, in: 2013 IEEE ICC in Budapest, Hungary, 2013, pp. 818–823. doi:10.1109/iccw.2013.6649346.

[25] A. Noel, K. C. Cheung, R. Schober, Improving receiver performance of diffusive molecular communication with enzymes, IEEE Trans. Nanobiosci. 13 (1) (2014) 31–43. doi:10.1109/tnb.2013.2295546.

[26] J. G. Proakis, Digital Communications 5th Edition, McGraw Hill, 2007.

[27] L. Nyholm, Electrochemical techniques for lab-on-a-chip applications, Analyst 130 (5) (2005) 599–605. doi:10.1039/B415004J.

[28] B. Dacorogna, Introduction to the Calculus of Variations, 3rd Edition, Imperial College Press, 2014.

[29] C. T. Crowe, J. D. Schwarzkopf, M. Sommerfeld, Y. Tsuji, Multiphase Flows with Droplets and Particles, 2nd Edition, CRC Press, 2011. doi:10.1201/b11103.

[30] G. Eslami, E. Esmaeilzadeh, A. T. Pérez, Modeling of conductive particle motion in viscous medium affected by an electric field considering particle-electrode interactions and microdischarge phenomenon, Phys. Fluids 28 (10) (2016) 107102. doi:10.1063/1.4964683.

[31] R. Wang, S. Sun, W. Wang, Z. Zhu, Investigation on the thermophoretic sorting for submicroparticles in a sorter with expansion-contraction microchannel, Int. J. Heat Mass Transfer 133 (2019) 912–919. doi:10.1016/j.ijheatmasstransfer.2018.12.126.

[32] W. Wicke, T. Schwering, A. Ahmadzadeh, V. Jamali, A. Noel, R. Schober, Modeling duct flow for molecular communication, in: 2018 IEEE Global Communications Conference (GLOBECOM), 2018, pp. 206–212. doi:10.1109/glocom.2018.8647632.

[33] M. Zoofaghari, H. Arjmandi, Diffusive molecular communication in biological cylindrical environment, IEEE Trans. Nanobiosci. 18 (1) (2018) 74–83. doi:10.1109/tnb.2018.2885051.

[34] Y.-F. Lo, C.-H. Lee, P.-C. Chou, P.-C. Yeh, Modeling molecular communications in tubes with Poiseuille flow and Robin boundary condition, IEEE Commun. Lett. 23 (8) (2019) 1314–1318. doi:10.1109/lcomm.2019.2920830.

[35] E. Antonopoulou, C. F. Rohmann-Shaw, T. C. Sykes, O. J. Cayre, T. N. Hunter, P. K. Jimack, Numerical and experimental analysis of the sedimentation of spherical colloidal suspensions under centrifugal force, Phys. Fluids 30 (3) (2018) 030702. doi:10.1063/1.5010735.

[36] S. L. Seyler, S. Pressé, Long-time persistence of hydrodynamic memory boosts microparticle transport, Phys. Rev. Res. 1 (2019) 032003. doi:10.1103/physrevresearch.1.032003.